Model Predictive Control of Active Suspension System on a Quarter Car Model

Hassan Sewailem (4673204), Zhehan Li (5217350)

***Abstract*—In this paper, the control problem of active suspension system of a quarter car model is formulated as the disturbance attenuation problem with hard constraints. Various Model Predictive Control (MPC) strategies are designed to improve the comfort for the passengers by attenuating road preview disturbance while meeting constraints dynamically. Based on Lyapunov stability theory, the asymptotic stability for the origin of the closed-loop linear state-measurement MPC system is proven. Simulation experiments show that the active suspension MPC strategy can increase 37.6% ride comfort compared to negative suspension system while satisfying the safety requirements.**

I. Introduction

Vertical vehicular motion caused by the irregular road surfaces resulting in disturbances does lead to discomfort for the passenger. How the passenger in the car feels the impact of the irregularity of the road surface is one of the critical factors in evaluating the quality of the vehicle. Although a certain level of vibration perception inside the car is accepted, the goal is to suppress the vertical vehicle motion to the point where the passenger stops having a feeling of discomfort, as the satisfaction of the passenger will add market value to the car.

Passive suspension systems can attenuate the disturbances up to a certain level due to constant mechanical configuration no matter what the amplitude of the disturbance is and what frequency range is the disturbance operating in. However, the active suspension system uses a controller (software) and an electromagnetic actuator system that produces a vertical force to suppress road disturbances based on a certain control law.

One limitation to the active suspension is the maximum actuator force constraint, which could limit to what level the disturbances are attenuated. In addition, the suspension has a limited stretching length and the tyre has a maximum compression, which could impose major safety risks if they are surpassed. This brings up the question: how to ensure tyre handling, suspension stability and comfort for the passengers in a vehicle by means of control of an active suspension systems while taking into account the limitations of the actuator.

In this paper, Model Predictive Control (MPC) methodology for an active suspension system is implemented on a model of a BMW 530i car, whose linear state-space representation will be summarized in section II, following the structure of the designed MPC controllers in section III. In section IV, the stability of the MPC solution will be assessed. Finally, the numerical simulations will be discussed in section V.

II. Active suspension system models

A. Road preview disturbance model

The main sources of vertical motion excitation is road, thus an accurate model that represents the road is key to performing accurate simulations of the car motion in the future.

The ISO 8608 [1] standard is used to model the road preview disturbance (road profile). The road roughness can be classified by calculating the power spectral density of the vertical displacement G_d (m^3) with respect to the spatial and the angular spatial frequencies n (cycles/m) and Ω (rad/m) respectively. There are 8 different classes of roads starting with "A" which represents the smoothest road, and ending with "H" which represents the roughest road where most disturbances occur. The values of $G_d(n_0)$, $G_d(\Omega_0)$, n_0 and Ω_0 for all road classes are adopted from [2].

There are two types of road profile in this paper: One of the methods to model the road profile is the vertical velocity road against time [3],

$$\dot{z}_0(t) = 2\pi\sqrt{G_d(n_0)V}\cdot\omega(t), \tag{1}$$

where ω is a Gaussian white noise signal with $E[\omega] = 0$ and $cov[\omega] = 1$ and V represents the speed of the car. Road class "C" was chosen as it represents what an average road would look like and two velocities, $V = 30km/hr$ and $V = 60km/hr$ were chosen for analysis.

Another type of road profile is simulating a bump road face. The shape of bump is described as [4]:

$$\dot{z}_{bump}(t) = \frac{A}{2}(1-cos\frac{2\pi V(t-t_0)}{L}), \quad t_0 \le t \le \frac{L}{V} \tag{2}$$

where A is the bump height, L is the bump length, V represents the speed of the car and t_0 is the starting time of the bump and t is the simulation time length.

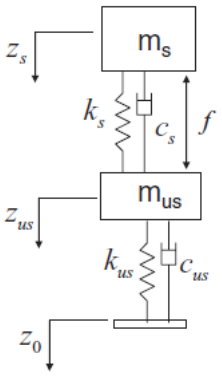

Fig. 1. Model of 2-DOF quarter car.

B. Quarter Car Model

The 2 degree of freedom quarter car model, presented in Fig.1, represents the vertical motion of a car regarding the reaction to road irregularities. It considers two stages of the car, the stage where there is sprung mass m_s (where the passengers are) and a second stage where the unsprung mass m_{us} (mass of suspension+tyre) is (see Fig.1).

The spring of the passive suspension system k_s is assumed to be parallel to the damper of the passive suspension system c_s, f_A represents the actuator force acting on m_s and m_{us}. Applying Newton's second law, the dynamic equations that govern the two-mass system are [5]:

$$\begin{cases} \mathrm{m}_s\ddot{z}_s + c_s(\dot{z}_s - \dot{z}_{us}) + k_s(z_s - z_{us}) = -f_A \\ \mathrm{m}_{us}\ddot{z}_{us} + c_s(\dot{z}_{us} - \dot{z}_s) + k_s(z_{us} - z_s) + c_{us}(\dot{z}_{us} - \dot{z}_0) + k_{us}(z_{us} - z_0) = f_A \end{cases} \tag{3}$$

Table I has the parameters for the model considered here, based on data for the BMW 530i car presented in [6]. In order to represent the states $x = \begin{bmatrix} z & \dot{z}_s & z_t & \dot{z}_{us} \end{bmatrix}^T$, input $u = \begin{bmatrix} f_A & \dot{z}_0 \end{bmatrix}^T$ and output $y = \begin{bmatrix} \ddot{z}_s & z & z_t \end{bmatrix}^T$, the linear state-space representation were derived as follows [3],

$$A = \begin{bmatrix} 0 & 1 & 0 & -1 \\ -\frac{k_s}{m_s} & -\frac{c_s}{m_s} & 0 & \frac{c_s}{m_s} \\ 0 & 0 & 0 & 1 \\ \frac{k_s}{m_u} & \frac{c_s}{m_u} & -\frac{k_t}{m_u} & -\frac{c_s}{m_u} \end{bmatrix}, \; B = \begin{bmatrix} 0 & 0 \\ -\frac{1}{m_s} & 0 \\ 0 & -1 \\ -\frac{1}{m_u} & 0 \end{bmatrix}$$
$$C = \begin{bmatrix} -\frac{k_s}{m_s} & -\frac{c_s}{m_s} & 0 & \frac{c_s}{m_s} \\ 1 & 0 & 0 & 0 \\ 0 & 0 & 1 & 0 \end{bmatrix}, \; D = \begin{bmatrix} \frac{1}{m_s} & 0 \\ 0 & 0 \\ 0 & 0 \end{bmatrix} \tag{4}$$

where z_s is the sprung mass elevation, z_{us} the unsprung mass elevation, z_0 the road elevation, $z = z_s - z_{us}$ the suspension stroke and $z_t = z_{us} - z_0$ the tyre deflection.

TABLE I
PARAMETERS OF THE QUARTER CAR MODEL(BMW 530I)

Symbol	Variable name	Value	Unit
m_s	Sprung mass	395.3	Kg
m_{us}	Unsprung mass	48.3	Kg
k_s	Spring stiffness	30.01e3	N/m
c_s	Spring damping	1450	Ns/m
k_{us}	Tyre Stiffness	3.4e5	N/m
c_{us}	Tyre Damping	0	Ns/m
f_{max}	Maximum actuator force	$\pm$2500	N
$z_{t,max}$	Maximum tyre deflection	$\pm$0.0128	m
z_{max}	Maximum suspension stroke	+0.09, -0.08	m

TABLE II
DISCOMFORT MEASURES

RMS of vertical acceleration $\ddot{z}_s$ (m/s^2)	Comment
< 0.315	Not uncomfortable
0.315-0.63	A little uncomfortable
0.5-1	Fairly uncomfortable
0.8-1.6	Uncomfortable
1.25-2.5	Very uncomfortable
> 2	Extremely uncomfortable

The discretization of the continuous state space matrices at a sampling time of 0.01s preserves the controllability and observability of the continuous time dynamics. The discretization method used was zero-order hold to simulate the usual DAC and ADC sensors typically used in these applications [7].

C. Ride Model

The ride model is one of the subjective factors that assess the car quality as it is mainly due to the perception of the passenger. According to the standard ISO 2631 [2], the level of comfort/discomfort can be assessed in terms of measurable quantities where an accurate evaluation can be made. The main parameter that can be used is the root mean square (RMS) of the vertical acceleration of the sprung mass $\ddot{z}_s$. As it can be seen in table II, no discomfort is caused when $\ddot{z}_s$ is less 0.315 m/s^2. Ultimately, the least discomfort rating possible would be the goal to achieve, however, if it is very difficult due to limitations in the actuator and the safety constraints, a little uncomfortable rating would be also acceptable.

III. MODEL PREDICTIVE CONTROL DESIGN

The vertical motion suppression of a vehicle is a multi-objective control problem in which MPC has the ability to solve. Based on the car dynamics presented in section II, three MPC strategies were designed to control the active suspension system.

A. Regulation MPC

In this case, full-state information is assumed, and the goal is to stabilize the discretized linear system as described in the Equation 4. The equilibrium at origin represents that the car is moving at a uniform speed on an absolutely level road with zero body vibration and zero tyre deflection. The cost function used to solve the MPC optimization problem at each iteration is represented as follow:

$$J(x_0, \mathbf{u}_N) = \frac{1}{2}\sum_{k=0}^{N-1}\{\ell(x(k), u(k))\} + V_f(x(N)) \\ s.t.\ \ \mathbf{u}_N \in \mathbb{U}, x \in \mathbb{X}, x(N) \in \mathbb{X}_f \tag{5}$$

with the stage and terminal costs defined as:

$$\ell(x(k), u(k)) = x(k)^T Q x(k) + u(k)^T R u(k) \tag{6}$$

$$V_f(x(N)) = \frac{1}{2} x(N)^T P x(N) \tag{7}$$

where Q = diag(0.1, 5, 0.1, 5), R = diag($10^{-7}, 10^{-7}$) and P solves the discrete-time Lyapunov equation $A_K^T P A_K = P - 2Q_K$, which would help the stability proof in section IV. Here, $A_K = A + BK$ with K the solution to the discrete-time algebraic Riccati equation for the matrices (A, B) and $Q_K = Q + K^T R K$.

The choices of Q and R were obtained following an iterative tuning procedure which could ensure a balance between control action and settling-time. This tuning procedure is demonstrated in subsection V-B. Note that Q, R and P are positive definite. Furthermore, the terminal set $\mathbb{X}_f$ was chosen properly to facilitate the stability proof in section IV.

The system inputs consist of the actuator force f_A and road preview disturbance $\dot{z}_0(t)$. Considering the actuator's output saturation, control variable constraint is $|f_A| \leq f_{Amax}$, where f_{Amax} = 2500N is the maximum actuator force in Table I. To show the asymptotically stable origin of the closed-loop linear system of regulation MPC in section IV, $\dot{z}_0(t)$ is assumed to be zero all the time. This is a reasonable assumption, as if the road preview disturbance persists over time, the system would repeatedly be kicked out of its equilibrium position. The input constraints $\mathbf{u}_N \in \mathbb{U}$ are therefore defined as

$$|f_A| = |\mathbf{u}_N(1:2:end)| \leq f_{Amax} \tag{8}$$

$$\dot{z}_0(t) = \mathbf{u}_N(2:2:end) == 0 \tag{9}$$

The state constraints of the quarter car model values are computed by taking average between front and rear wheel values [5]:

$$m = \begin{bmatrix} -0.044 \\ -0.163 \\ -0.015 \\ -1.965 \end{bmatrix} \leq \begin{bmatrix} z_s - z_u \\ \dot{z}_s \\ z_t \\ \dot{z}_{us} \end{bmatrix} \leq \begin{bmatrix} 0.0525 \\ 0.14 \\ 0.029 \\ 2.78 \end{bmatrix} = M \tag{10}$$

The state constraints $x \in \mathbb{X}$ can now be represented compactly as $Fx(k) \leq e$, where F and e are given by:

$$F = [I\ \ -I]^T;\ \ e = [M\ m]^T \tag{11}$$

Since the MPC problem is ultimately an optimization on the control inputs, the state constraints $x \in \mathbb{X}$ are related to the input constraints by using the prediction relationship

$$x_{N+1} = Tx_0 + S\mathbf{u}_N \tag{12}$$

where the details of T and S are provided in Appendix Equation 24 . The state constraints are therefore defined as

$$F(Tx_0 + S\mathbf{u}_N) \leq e \rightarrow \mathbf{u}_N \leq (FS)^{-1}(e - FTx_0) \tag{13}$$

When making the choice of the prediction horizon N, several factors need to be taken into account: controllability needs to be ensured along with making sure that the MPC problem is not too computationally expensive. After some manual tuning, a value of N = 6 was chosen as it satisfied both conditions.

B. Offset free output feedback MPC with state observer

In reality, full state-measurements are unavailable. To simulate output-based control, an output MPC controller was designed to simulate limited direct access to state information via sensor hardware. As (A, C) is an observable pair, the states can be reconstructed using a state observer. The state-equation of the observer is given by:

$$\tilde{x}^+ = (A - LC)\tilde{x} + Bu + Ly \tag{14}$$

with the matrix L chosen to be the Kalman observer gain with process and measurement covariance matrices set to identity matrices. In a real experiment, iterative tuning of the weighting matrices would be required to ensure adequate noise filtering. In this case, they are chosen to ensure the observer error converges faster to zero than the closed-loop system.

The disturbance d is assumed to be known and is added to the state-space system, resulting in the following new state-space system

$$x^+ = Ax + Bu + B_d d \quad\ \ y = Cx + Du + C_d d \tag{15}$$

where $d = \begin{bmatrix} -0.1 \\ 0.1 \end{bmatrix}$, $B_d = \begin{bmatrix} 1 & 0 \\ 0 & 1 \\ 1 & 0 \\ 0 & 1 \end{bmatrix}$, $C_d = \begin{bmatrix} 1 & 0 \\ 0 & 1 \\ 1 & 0 \end{bmatrix}$. In order to reject disturbance d in the closed-loop system, an augmented state-space system is required, which can be used to estimate the disturbance acting on the system in order to counter them as explained in Section 5.5 of [8]. The augmented state-space system is represented by

$$\begin{bmatrix} x^+ \\ d^+ \end{bmatrix} = \begin{bmatrix} A & B_d \\ 0 & I \end{bmatrix} \begin{bmatrix} x \\ d \end{bmatrix} + \begin{bmatrix} B \\ 0 \end{bmatrix} u \tag{16}$$

$$y = \begin{bmatrix} C & C_d \end{bmatrix} \begin{bmatrix} x \\ d \end{bmatrix} + Du \tag{17}$$

In order to ensure the augmented system is observable, it is required that the original system (A,C) is observable as well as

$$rank \begin{bmatrix} I - A & -B_d \\ C & C_d \end{bmatrix} = n_x + n_d \tag{18}$$

where Equation 18 is satisfied with $n_x + n_d$ = 7. In addition, the road preview disturbance $\dot{z}_{bump}(t)$ was also applied to the augmented system as the second time-varying input value.

For reference tracking and disturbance rejection, an optimal target selection (OTS) needs to be solved online to obtain the required x_{ref} and u_{ref} to reject disturbances on x and y. The OTS problem to be solved at each iteration is described as follow

$$(x_{ref}, u_{ref})(\tilde{d}, y_{ref}) \in \begin{cases} arg\ min_{x_r, u_r} J(x_r, u_r) \\ s.t. \\ \begin{bmatrix} I - A & -B \\ C & D \end{bmatrix} \begin{bmatrix} x_r \\ u_r \end{bmatrix} \\ = \begin{bmatrix} 0 \\ y_{ref} - \tilde{d} \end{bmatrix} \\ (x_r, u_r) \in \mathbb{Z} \\ Cx_r + Du_r + \tilde{d} \in \mathbb{Y} \end{cases} \tag{19}$$

With the references x_{ref} and u_{ref} solved using the OTS at each iteration, the stage and terminal costs are just adjusted to account for the reference signals as follow

$$\begin{aligned} \ell(x(k), u(k)) &= (x(k) - x_{ref})^T Q (x(k) - x_{ref}) \\ &\quad + (u(k) - u_{ref})^T R (u(k) - u_{ref}) \\ V_f(x(N)) &= \frac{1}{2} (x(N) - x_{ref})^T P (x(N) - x_{ref}) \end{aligned} \tag{20}$$

Following a similar procedure as described for the regulation MPC design, the cost weighting matrices were chosen to be $Q = I$, $R = 0.001I$ and P is the solution to the DARE of the unconstrained problem. Finally, the prediction horizon N was selected to be 6 for the same reasons as explained in the regulation MPC design.

C. Adaptive MPC for Time-varying Disturbance

In this section, Adaptive MPC will be performed on the quarter-car model of the linear state-space in Equation 4 . With the road preview disturbance $\dot{z}_0(t, K, V)$ depending on road class K and speed of the car V being updated per prediction step t, the control strategy is to find the maximum speed V using a velocity update iteration, which makes the optimization feasible and satisfy all the hard constraints to ensure comfort and tire safety.

The key objective for ride comfort enhancement is to penalize and suppress the output y being the sprung mass acceleration $\ddot{z}_s$ (comfort), the tyre deflection z_t (safety) and the suspension stroke $z_s - z_u$ (safety) while satisfying the actuator limits. For this reason the cost function will be written in terms of y, having input constraints and additional output constraints, to ensure that the passenger comfort and safety do not surpass a certain limit that is undesirable. Therefore the Adaptive MPC is an output-penalized optimization strategy.

In order to transform the output constraints into the input constraints, an output prediction model is required, where the output sequence is decided by the initial state and control input sequence. Note that we assume that the full state-measurements are available in this case and there is no extra sensor noise. Equation 12 is rewritten in matrix form as below

$$Y_N = \Gamma x_0 + \Phi \mathbf{u}_N \tag{21}$$

The details of deriving Γ and Φ are provided in Appendix Equation 25 .

The objective function for Adaptive MPC is defined:

$$\begin{aligned} J(x_0, \mathbf{u}_N) &= \frac{1}{2} \sum_{k=0}^{N-1} (y(k) - y_{ref})^T Q (y(k) - y_{ref}) \\ &\quad + u(k)^T R u(k) = \frac{1}{2} \mathbf{u}_N^T H \mathbf{u}_N + h^T \mathbf{u}_N + c \\ &s.t.\ \ \mathbf{u}_N \in \mathbb{U}, x \in \mathbb{X}, y \in \mathbb{Y} \end{aligned} \tag{22}$$

where $H = \Phi^T \bar{Q} \Phi + \bar{R}$, $h = \Phi^T \bar{Q} \Gamma x_0$. The derivation of H and h are provided in Appendix Equation 26. Through simulation experiments, the R matrix is set as a zero matrix ($R =$ **zeros**$(dim.n_u, dim.n_u)$=**zeros**$(2, 2)$), which can obtain a significant control effect [9]. The Q matrix equals to **diag**(0.1, 0.0001, 0.0001), which is chosen such that $\ddot{z}_s$, the direct indicator of the uncomfort,

is penalized harshly, $z_s - z_u$ and z_t, the indicator of the tyre unsafety, are penalized softly. Since the output of the vehicle is expected to be same as the stationary output during the braking process, the output reference y_{ref} is set as **zero**(3,1). The output constraints $y \in \mathbb{Y}$ can be designed based on the comfort and safety requirements.

When the speed of the car V decreases, the vibration of the sprung mass decreases, and passengers feel more comfortable. When the car speed is too high, the above optimization problem may become infeasible because the output or input constraints cannot be satisfied. In order to ensure that the optimization problem is feasible on the one hand, and to obtain the highest speed on the other hand, a feasible speed update iteration is used outside the MPC optimization iteration.

IV. Asymptotic stability

In this section, the designed regulation MPC controller in subsection III-A is shown to asymptotically stabilize the closed-loop system provided the system's initial conditions are sufficiently close to the origin.

We will follow the approach of Section 2.5.4 of [8], by proving the satisfaction of Assumption 2.2, 2.3, 2.14 and 2.17 in [8], and ultimately result in the statement that Theorems 2.19 and 2.21 in [8] can be used to show that the origin of the linear system is exponentially stable in $\mathcal{X}_N$. It will be verified by simulations in subsection V-C that the proposed Output MPC is also able to stabilize the closed-loop system with the bump road preview disturbance $\dot{z}_{bump}$, but as this is not the main goal of the paper, stability for Output MPC will not be proven. The following sub-sections in this section are the procedures of proving assumptions required.

A. Estimating $\mathbb{X}_f$ and $\mathcal{X}_N$

The goal of this sub-section for proving stability is to estimate the maximum invariant constraint admissible set $\mathbb{X}_f$ and the region of attraction $\mathcal{X}_N$ such that initial conditions starting in $\mathcal{X}_N$ will be guaranteed to converge towards the origin asymptotically.

$\mathbb{X}_f$ is the set which ensures the MPC optimal control input will be the same as the unconstrained control input defined by the infinite-horizon LQR problem. Within this set $\mathcal{K}_N(x) = Kx$ where K is the optimal LQR gain. Using Algorithm 1 presented in [10], an invariant set $\mathbb{X}_f$ can be estimated which adheres to the control input and state constraints stated in Equation 8 and Equation 11. The $\mathbb{X}_f$ is found to contain 23 linear inequalities represented by $Jx \leq j$, which can be formally defined as

$$\mathbb{X}_f = \{x \in \mathbb{R}^4 | Jx \leq j\} \tag{23}$$

With an estimation of $\mathbb{X}_f$, an empirical analysis is done to reconstruct $\mathcal{X}_N$. This is done by considering a large set of initial conditions x_0 and checking the feasibility of the MPC problem with the terminal constraint $x(N) \in \mathbb{X}_f$. If the problem is feasible, x_0 lies in $\mathcal{X}_N$. Based on Algorithms 2 and 3 in [10], a 2-D plot of $\mathcal{X}_N$ is obtained as the last figure in the corresponding MATLAB code.

B. Assumption 2.2

In this section, the Assumption 2.2 underlying Theorem 2.19 and 2.21 of [8] is proven. The system description in Equation 4 is linear, which means it is continuous and has an equilibrium point as (x,u)=(0,0). The stage cost in Equation 6 and terminal cost in Equation 7 are continuous, positive definite functions, and $\ell(0,0) = 0$ and $V_f(0,0) = 0$, as they are quadratic functions with Q,R,P $\succ 0$. It also follows that $\ell(x,u) = x^TQx + u^TRu \geq x^TQx \geq \lambda_{min}(Q)|x|^2 = c_1|x|^a$, with $c_1 = \lambda_{min}(Q)$ and $a = 2$. Similarly, we have $V_f(x) = \frac{1}{2}x^TPx \leq \frac{1}{2}\lambda_{max}(P)|x|^2 = c_2|x|^a$, and $V_f(x) \geq \frac{1}{2}\lambda_{min}(P)|x|^2 = c_3|x|^a$, with $c_2 = \frac{1}{2}\lambda_{max}(P)$, $c_3 = \frac{1}{2}\lambda_{min}(P)$ and $a = 2$ as well. This also implies that the cost functions are class $\mathcal{K}_\infty$ functions because they are norm functions, zero at origin, strictly increasing and radially unbounded, which also proves Assumption 2.17 in [8] (Assumption 2.17 can also be verified by the system being controllable).

C. Assumption 2.3

To verify if Assumption 2.3 of [8] holds, we recall from subsection III-A that all states x and the control action u have been upper and lower bounded through Equation 11 and Equation 8 and Equation 9. Therefore these constraints $\mathbb{X}$ and $\mathbb{U}$ both are closed, compact and contain the origin in its interior, that is $0 \in int(\mathbb{X})$ and $0 \in int(\mathbb{U})$. Similarly, since $\mathbb{X}_f \subseteq \mathbb{X}$, the terminal set $\mathbb{X}_f$ is bounded through linear inequalities in Equation 23. Thus it follows that $\mathbb{X}_f$ is closed and bounded sets. By the Heine-Borel theorem, $\mathbb{X}_f$ is compact sets. Furthermore, $\mathbb{X}_f$ contains the origin in its interior $0 \in int(\mathbb{X}_f)$.

D. Assumption 2.14

For the stability proof, one of the key assumptions is the control invarinace and a Lyapunov decrease within the terminal set as stated in Assumption 2.14 in [8]. The assumption is verified if $\forall x \in \mathbb{X}_f, \exists u \in \mathbb{U}\ s.t. f(x,u) \in \mathbb{X}_f\ and\ V_f(f(x,u)) - V_f(x) \leq -\ell(x,u)$.

With $u = Kx$ and the notation introduced in subsection III-A, the above assumption reduces to

$V_f(A_K x) \leq V_f(x) - \frac{1}{2}x^T Q_K x$. Note that $V_f(A_K x) = \frac{1}{2}(A_K x)^T P(A_K x) = \frac{1}{2}x^T A_K^T P A_k x$. As P solves the equation $A_K^T P A_K^T = P - 2Q_K$, we have (based on Q is positive definite):

$$V_f(A_K x) = \frac{1}{2}x^T Px - x^T Q_K x \leq \frac{1}{2}x^T Px - \frac{1}{2}x^T Q_K x = V_f(x) - \ell(x,u)$$

The Lyapunov decrease is thus proven for an initial condition with $\mathbb{X}_f$.

Additionally, the assumption that $\mathbb{X}_f$ is invariant is also confirmed by considering the state trajectories and ensuring a posteriori that there exists a $u((x,u) \in \mathbb{Z})$ satisfying all states within $\mathbb{X}_f$ remaining in $\mathbb{X}_f$ using the $Jx \leq j$ inequality obtained in Equation 23. In section subsection V-B, with initial states within $\mathbb{X}_f$, the state trajectories of MPC are shown to be within the $\mathbb{X}_f$ and converges to origin in the end.

Assumption 2.14(a) is proven above, and (b) holds as discussed for Assumption 2.2.

V. Numerical Simulations

In this section, simulations are carried out using the MPC design from section III. First, simulations of the influence of the horizon length N and the weighting matrices Q, R to the regulation MPC performance will be analysed. The stability convergence of the regulation MPC with different initial states conditions and different road preview disturbance will be researched as well. Next, simulations of the offset free output feedback MPC with state observer and disturbance rejection will be shown. Finally, the adaptive MPC with real world road profile will be implemented on the linear model, to be compared with the negative suspension system controller in terms of comfort and safety.

A. Regulation MPC: Prediction Horizon N

Figure 2 shows the system state trajectories for different prediction horizons. In order to show that the regulation MPC can stabilize the system again when the system experiences disturbance after reaching the equilibrium point, a bump road preview disturbance $\dot{z}_{bump}$ is implemented at simulation steps 100. By observation, the system is unstable for N=2 before and after the disturbance $\dot{z}_{bump}$ because most of the states are not converging to the origin. The choice for N=4 clearly shows a stable response. Despite minimal difference in the response for N=6, 8 and 15, a larger N ensures a larger region of attraction $\mathcal{X}_N$ but higher computational demands. Therefore, the prediction horizon was kept for N=6.

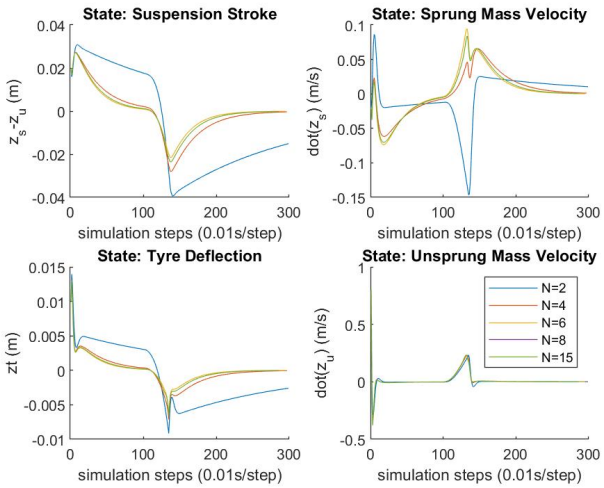

Fig. 2. System state response for different prediction horizons N

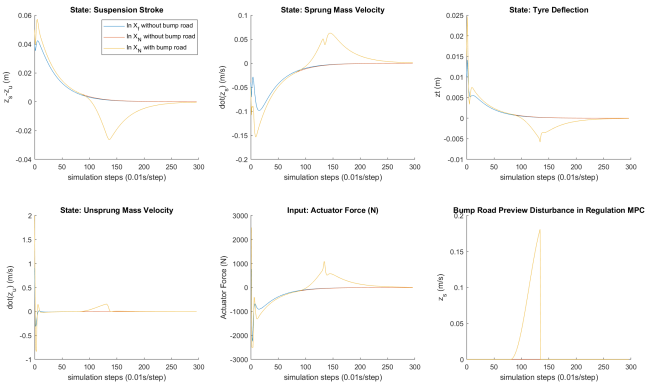

Fig. 3. Asymptotic convergence of the state trajectories in three cases

B. Regulation MPC: Weighting Matrices Q & R

In this sub-section, the regularizing MPC controller is used to illustrate the effect different cost function choices have on the closed-loop system's performance. To begin with, Figure 3 shows the states refectories converging to the origin with different initial condition $x_0 \in \mathbb{X}_f$ or $x_0 \in \mathcal{X}_N$ and with or without the road disturbance $\dot{z}_{bump}$.

Figure 4, Figure 5 shows the states trajectories of the closed-loop system using various Q and R weighting matrices used in the MPC cost functioon as defined in Equation 6 respectively. Figure 6 shows the input actuator force trajectories of the regulation MPC with different R matrices in Figure 5. From Figure 4 we can observe that small Q value requires longer settling times but guarantees that all the states converge to origin in the end. However, with larger Q values, the state trajectories are staying in $\mathbb{X}_f$ but not converging to the origin. This could be explained by the fact that for larger

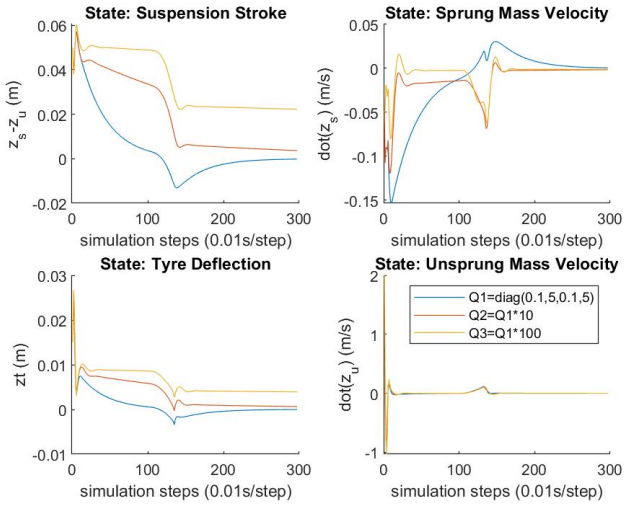

Fig. 4. State trajectories for different stage cost matrices Q with R=R1, N=6.

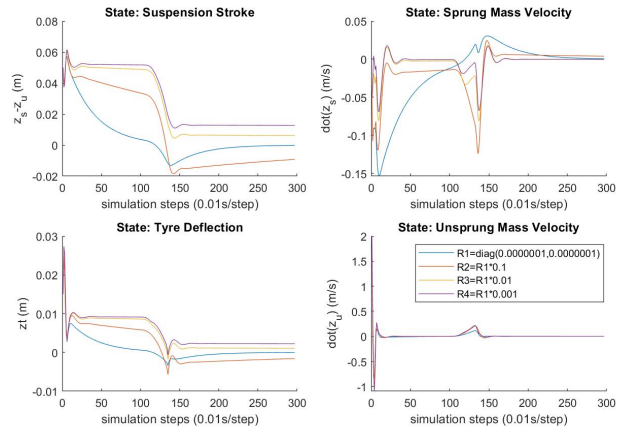

Fig. 5. State trajectories for different stage cost matrices R with Q=Q1, N=6.

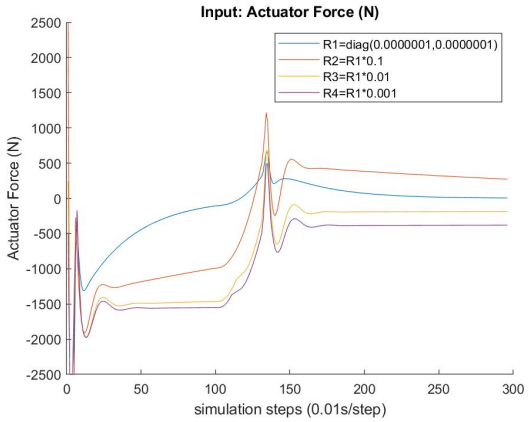

Fig. 6. Input Actuator force trajectories for different state cost matrices R with Q=Q1, N=6.

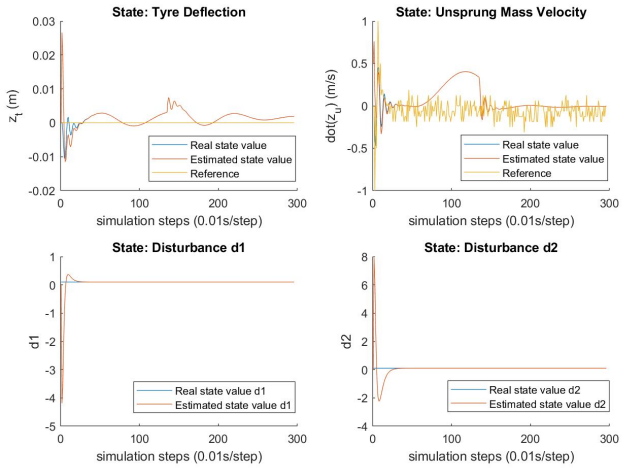

Fig. 7. Reference (from OTS) tracking, disturbance d estimation and road disturbance $\dot{z}_{bump}$ rejection. $\dot{z}_{bump}$ is active starting at 0.8 sec.

Q values, larger inputs are required to ensure the smaller state errors, but the input constraints prevent this from happening, resulting in state offsets.

On the other hand, from Figure 5 and Figure 6, we can observe that with smaller R value the absolute value of the maximum applied actuator force increases and converges to a higher value in the end. However, with smaller R value, the state trajectories are staying in $\mathbb{X}_f$ but not converging to the origin. This could be explained by the fact that for smaller R values, the applied inputs are too large to force the system to reach the equilibrium point.

C. Output MPC and Disturbance Rejection using Observer

Assuming we only have access to the output measurements of the suspension system, we can use an observer to reconstruct the states for use in MPC control. As datailed in Equation 17, this observer is augmented with a disturbance observer to simulate a constant lateral offset acting on the suspension system.

Figure 7 shows a simulation where a disturbance $d = [d1; d2] = [0.1; 0.1]$ is acting on the system and a bump road preview disturbance $\dot{z}_{bump}$ active from 0.8 second. The figure shows how the output MPC controller manages to estimate d, reject the $\dot{z}_{bump}$ and d disturbance, and track the state reference obtained from OTS with $y_{ref} = [0; 0; 0]$ in Equation 19. Note the settling time of the observer on the disturbance d and states of approximately 0.13 second, which is considerably faster than the system's settling time of approximately 1 second, implying the observer gains were well chosen.

D. Comfort and safety analysis: Adaptive MPC

In this subsection, the Adaptive MPC controller performance will analysed based on how well the comfort and safety objectives for the passengers are achieved at speeds $V = 30$ km/hr and $V = 60$ km/hr. The performance will then be compared with the case where there is only passive suspension acting on the quarter-car model.

1) $V = 30$ km/hr: Starting with the case where only passive suspension is acting, it can be noticed from Fig.8 that at $V = 30km/hr$, comfort is not satisfied with the sprung mass acceleration $\ddot{z}_s$ having an RMS value of $0.8812\ m/s^2$ which puts the comfort level to the "uncomfortable" rating in Table.II whereas safety is achieved having satisfied the suspension stroke z_{max} and the tyre deflection $z_{t,max}$ constraints in Table.I. On the other hand, when adaptive MPC is applied along with the passive suspension, comfort performance significantly improves. Looking at Fig.9, it can realised that the RMS of $\ddot{z}_s$ reduces by 37.6 % having an RMS value of $0.55\ m/s^2$ which puts the discomfort level in the "A little uncomfortable" to "fairly uncomfortable" range which is desirable. The safety objectives are also satisfied having satisfied the constraints in Table.I. The actuator force, in Fig.9 has a peak magnitude of $f_{A,max} = 1217.6$ N at $V = 30$ km/hr, which satisfies the actuator limitations in Table.I. The RMS actuator force in this case has a magnitude of 333.7 N.

2) $V = 60$ km/hr: When the velocity of the car is higher, at $V = 60$ km/hr, intuitively, it is safe to say comfort is more difficult to achieve. This can be reflected on the case where the passive suspension system is only acting, where it can be seen in Fig.8 that at $V = 60$ km/hr $\ddot{z}_s$ has increased with higher magnitude fluctuations having an RMS value of 1.25 m/s^2, 1.42 times higher than at $V = 30$ km/hr. This puts the discomfort rating at "uncomfortable" to "very uncomfortable". Safety objectives for z and z_t are satisfied which can be seen on Fig.8. When MPC is applied, comfort performance has improved which can be seen in Fig.9, where at $V = 60$ km/hr, $\ddot{z}_s$ fluctuates at lower magnitudes having an RMS value of $1.0438\ m/s^2$, 16.42 % lower than the case where only passive suspension is acting reduces the discomfort to the "uncomfortable" rating. Safety objectives are still maintained as seen in Fig.9 and the peak actuator for had a magnitude $f_{A,max} = 1479.5$ N, satisfying the actuator limitations in Table.I. In this case, the actuator force has an RMS value of 259 N, 1.29 times lower than for the case of $V = 30$ km/hr.

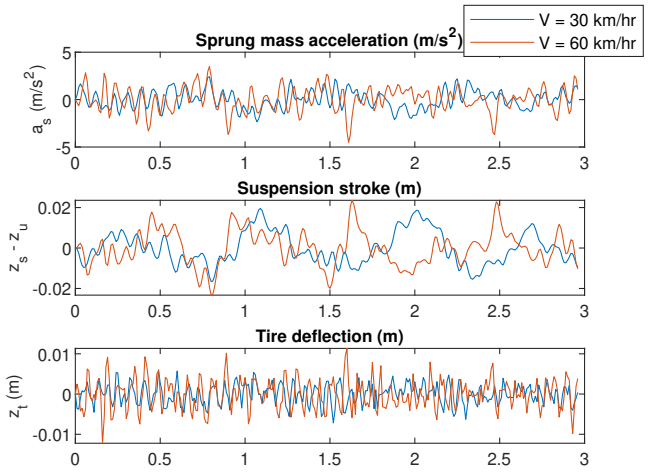

Fig. 8. Plots of $\ddot{z}_s$ (m/s^2), $z = z_s - z_u$ (m) and z_t (m) against time (s) at $V = 30$ km/hr and $V = 60$ km/hr, when the time-varying road input is applied with only passive suspension included.

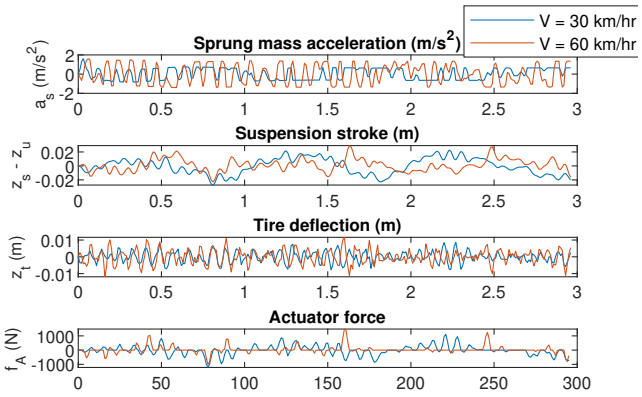

Fig. 9. Plots of $\ddot{z}_s$ (m/s^2) , $z = z_s - z_u$ (m), z_t (m) and the actuator force f_A against time (s) at $V = 30$ km/hr and $V = 60$ km/hr, when the time-varying road input is applied with passive and active (MPC) suspension included.

3) Discussion: It is evident that at lower speeds, the MPC controller performs better since the percentage improvement in comfort between active and passive suspension is significantly higher at speed $V = 30$ km/hr. This is due to the fact that the controller has more freedom to act at lower speeds which is the reason for the higher RMS of f_A at $V = 30$ km/hr as seen in Fig.9. The higher controller freedom is a consequence of the constraint on the tyre deflection z_t in Table.I, where at $V = 30$ km/hr, its maximum magnitude is around 0.007 m representing 54.7 % of $z_{t,max}$ (Table.I) whereas at $V = 60km/hr$, its maximum magnitude is 0.01 m, representing 78.1 % of $z_{t,max}$ when only passive suspension is acting. As a result, the main bottleneck is the tyre deflection, thus better quality tyres are needed for improved comfortability at higher speeds. The

suspension stroke was not mentioned as it is well within the limitations (see Table.I) and does not impose any significant limitations on the actuator force.

CONCLUSION

Models for the road using ISO 8608, 2 DOF quarter car and comfort using ISO 2631 were implemented using MATLAB in order to perform control design using different MPC strategies for an active suspension system on BMW 530i car model. The main objective was ensuring safety and comfort for the car passengers. The asymptotic stability of the region of the closed-loop linear system was guaranteed by using the designed regulation MPC. Through simulation, the output MPC was able to track the state references and reject the disturbances properly. Active-suspension system using adaptive MPC can achieve 37.6% comfort improvement and meet all safety requirements.

REFERENCES

[1] International Standard Organization, C. d. B., Mechanical vibration — Road surface profiles — Reporting of measured data , 2016, pp. 17–25.

[2] Standard, I., Mechanical vibration and shock - Evaluation of human exposure to whole body vibration - Part one *Journal of Magnetism and Magnetic Materials*, 1997.

[3] Yu, S., Xu, M., Sun, X., Qu, T., Zhuang, Y., and Chen, H., Model predictive control of magneto-rheological damper semi-active suspension with preview *2020 Chinese Automation Congress (CAC)*, 2020.

[4] H. Chen, K. G., Constrained H-infinity control of active suspensions: an lmi approach *The 2002 International Conference on Control and Automation, 2002. ICCA. Final Program and Book of Abstracts.*, Vol. 13, 2005, pp. 412–421.

[5] Ali G. Ulsoy, M. C., Huei Peng, *Automotive control systems*, Cambridge Univ. Press, United states of America, 2012.

[6] T.p.j.Van Der Sande, E., B.l.j.Gysen, Robust control of an electromagnetic active suspension system: Simulations and measurements *Mechatronics*, Vol. 23, 2013, pp. 204–212.

[7] Mo, C., and Sunwoo, M., A semiactive vibration absorber (SAVA) for automotive suspensions *International journal of vehicle design*, Vol. 29, No. 1-2, 2002, pp. 83–95.

[8] J.Rawling, and D.Mayne, Model Predictive Control Theory and Design, Nob Hill Publishing , 2008.

[9] Nguyen, M.-Q., Canale, M., Sename, O., and Dugard, L., A Model Predictive Control approach for semi-active suspension control problem of a full car *2016 IEEE 55th Conference on Decision and Control (CDC)*, IEEE, 2016, pp. 721–726.

[10] Sergio Grammatico, M. B., and Franci, B., Exercise set 4 of course "Model Predictive Control" (SC42125) in DCSC, TUDelft , 2021.

APPENDIX

$$
\begin{aligned}
X_{N+1} &= \begin{bmatrix} x(0) \\ x(1) \\ .. \\ x(N) \end{bmatrix} \\
&= \underbrace{\begin{bmatrix} I \\ A \\ .. \\ A^N \end{bmatrix}}_{T(N)} x_0 + \underbrace{\begin{bmatrix} 0 & 0 & .. & 0 \\ B & 0 & .. & 0 \\ .. & .. & .. & .. \\ A^{N-1}B & A^{N-2}B & .. & B \end{bmatrix}}_{S(N)} \underbrace{\begin{bmatrix} u_0 \\ u_1 \\ .. \\ u_{N-1} \end{bmatrix}}_{\mathbf{u}_N}
\end{aligned} \tag{24}
$$

$$
\begin{aligned}
Y_N &= \begin{bmatrix} y(0) \\ y(1) \\ .. \\ y(N-1) \end{bmatrix} = C. * X_N + D. * \mathbf{u}_N \\
&= C. * [T(N-1)x_0 + S(N-1)\mathbf{u}_N] + D. * \mathbf{u}_N \\
&= C. * T(N-1)x_0 + [C. * S(N-1) + D * I_N]\mathbf{u}_N \\
&= \underbrace{\begin{bmatrix} C \\ CA \\ .. \\ CA^{N-1} \end{bmatrix}}_{\Gamma} x_0 + \underbrace{\begin{bmatrix} D & 0 & .. & 0 \\ CB & D & .. & 0 \\ .. & .. & .. & .. \\ CA^{N-1}B & CA^{N-2}B & .. & D \end{bmatrix}}_{\Phi} \mathbf{u}_N
\end{aligned} \tag{25}
$$

$$
\begin{aligned}
&J(x_0, \mathbf{u}_N) \\
&= \frac{1}{2}\sum_{k=0}^{N-1} (y(k) - y_{ref})^T Q (y(k) - y_{ref}) + \mathbf{u}_N(k)^T R \mathbf{u}_N(k) \\
&= \frac{1}{2}\sum_{k=0}^{N-1} (\Gamma_{(k)} x_0 + \Phi_{(k)}\mathbf{u}_N(k))^T Q (\Gamma_{(k)} x_0 + \Phi_{(k)}\mathbf{u}_N(k)) \\
&+ \mathbf{u}_N(k)^T R \mathbf{u}_N(k) \\
&= \frac{1}{2}\sum_{k=0}^{N-1} \mathbf{u}_N(k)^T (\Phi_{(k)}^T Q \Phi_{(k)} + R)\mathbf{u}_N(k) \\
&+ (x_0^T \Gamma_{(k)}^T Q \Phi_{(k)})\mathbf{u}_N(k) + \mathbf{u}_N(k)^T (\Phi_{(k)}^T Q \Gamma_{(k)} x_0) \\
&+ x_0^T (\Phi_{(k)}^T Q \Phi_{(k)}) x_0 = \frac{1}{2}\mathbf{u}_N^T H \mathbf{u}_N + h^T \mathbf{u}_N + c \\
&H = \Phi^T \bar{Q} \Phi + \bar{R} \\
&h = \Phi^T \bar{Q} \Gamma x_0 \\
&c = \frac{1}{2} x_0^T \Gamma^T \bar{Q} \Gamma x_0 \\
&\bar{Q} = \begin{bmatrix} Q & .. \\ .. & Q \end{bmatrix}, \bar{R} = \begin{bmatrix} R & .. \\ .. & R \end{bmatrix}
\end{aligned} \tag{26}
$$